Vortex-core order and field-driven supersolidity

Madhuparna Karmakar,* Gautam I. Menon,† and R. Ganesh‡
Institute of Mathematical Sciences, HBNI, CIT Campus, Chennai 600 113, India
(Received 14 May 2017; revised manuscript received 20 September 2017; published 1 November 2017)

Superconductivity occurs in the proximity of other competing orders in a wide variety of materials. Such competing phases may reveal themselves when superconductivity is locally suppressed by a magnetic field in the core of a vortex. We explore the competition between superconductivity and charge density wave order in the attractive Hubbard model on a square lattice. Using Bogoliubov–de Gennes mean-field theory, we study how vortex structures form and evolve as the magnetic flux is tuned. Each vortex seeds a charge density wave region whose size is determined by the energy cost of the competing phase. The vortices form a lattice whose lattice parameter shrinks with increasing flux. Eventually, their charge-ordered cores overlap, leading to a field-driven coexistence phase exhibiting both macroscopic charge order and superconductivity—a "supersolid." Ultimately, superconductivity disappears via a first-order phase transition into a purely charge-ordered state. We demonstrate that the Hubbard model maps to a strong-coupling field theory with a constant-squared-sum constraint. We argue that such a constraint necessarily leads to ordered-vortex cores and field-driven coexistence. The coexistence phase can be interpreted as a crystalline arrangement of meron defects in a pseudospin description. We construct a phase diagram using t', the next-nearest-neighbor hopping, to tune the competition between phases.

DOI: 10.1103/PhysRevB.96.174501

I. INTRODUCTION

Superconductivity is often obtained in proximity to other ordered ground states. The most prominent example is the high-T_c cuprate family, where superconductivity competes with antiferromagnetism and with charge order [1,2]. A particularly interesting way to stabilize underlying competing phases is to apply a magnetic field, locally suppressing superconductivity to create vortices. The core region of the vortex can then host competing correlations [3–5]. Indeed, experiments with scanning tunneling microscopy have revealed charge-ordered [3,5] vortex cores in the cuprates. NMR studies of $YBa_2Cu_3O_y$ indicate that as the magnetic field increases, the intervortex distance decreases; at a critical field strength, vortex cores overlap leading to charge order throughout the system [6]. These and related experiments motivate the study of vortex core order and field-driven coexistence in the attractive Hubbard model, the simplest model to show competition between superconductivity (SC) and charge density wave (CDW) order.

II. HUBBARD MODEL AND $SO(3)$ SYMMETRY

We consider fermions on a square lattice, described by

$$H = \sum_{\langle ij\rangle,\sigma} \{-t_{ij} c^{\dagger}_{i,\sigma} c_{j,\sigma} + \text{H.c.}\} - U \sum_i \hat{n}_{i,\uparrow}\hat{n}_{i,\downarrow} - \mu \sum_{i,\sigma} \hat{n}_{i,\sigma}, \quad (1)$$

where t_{ij} denotes hopping, μ is the chemical potential, and U is the strength of the on-site attraction ($U > 0$). A remarkable symmetry emerges when the hopping is restricted to nearest neighbors and μ is tuned to half filling: SC and CDW orders become degenerate. Moreover, an enlarged $SO(3)$ vector order parameter emerges which has SC and CDW as its components, as shown in Fig. 1 (left) [7–11]. This is a delicate symmetry arising from the bipartite nature of the square lattice with hoppings connecting sites of different sublattices. We can tune away from this $SO(3)$ degenerate point by introducing a next-nearest-neighbor hopping, t'. The t' term lowers the energy of the SC phase relative to the CDW phase (see Fig. 7 in the Appendix).

The $SO(3)$ degeneracy leads to a pseudospin description with components $\{\text{Re}(\Delta_i),\text{Im}(\Delta_i),\tilde{\phi}_i\}$, as shown in Fig. 1. Here, Δ_i and $\tilde{\phi}_i$ (defined below) are the local SC and CDW order parameters. This $SO(3)$ symmetry is directly analogous to the hypothesized $SO(5)$ symmetry [12] in the cuprates which groups SC and antiferromagnetism into an enlarged order parameter space. As a testable consequence of $SO(5)$ theory, it was proposed that vortex cores would have antiferromagnetic order [13,14]. Analogously, the Hubbard model in Eq. (1) will possess CDW order in the vortex core. In the language of $SO(3)$ pseudospins, a vortex corresponds to a "meron," as shown in Fig. 1 (right); in the core region, the moments cant out of the plane to locally give rise to CDW order.

III. STRONG-COUPLING FIELD THEORY

Our first key result is that the Hubbard model, in the vicinity of the $SO(3)$-symmetric point, maps onto a field theory characteristic of phase competition. It is well known that at large U, the Hubbard model reduces to a spin problem with antiferromagnetic superexchange interactions [10,11]. The local order parameter is, in fact, the $SO(3)$ spin whose components are $\{\text{Re}(\Delta_i),\text{Im}(\Delta_i),\tilde{\phi}_i\}$ as shown in Fig. 1. We may expect the ground state to have uniform spin length, i.e., $|\Delta_i|^2 + \tilde{\phi}_i^2 = c$, a constant independent of position. This is a strong constraint on SC and CDW order parameters which can no longer fluctuate independently [13]. With these

*madhuparna.k@gmail.com
†menon@imsc.res.in
‡ganesh@imsc.res.in

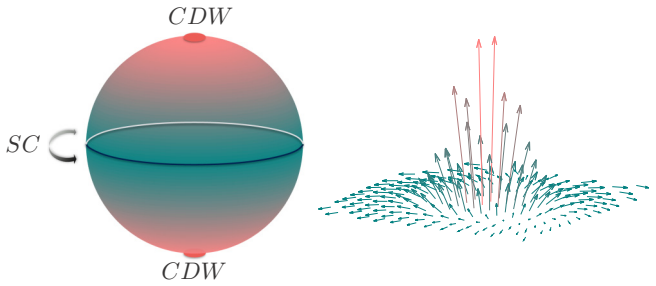

FIG. 1. Left: The space of order parameters forming an $SO(3)$ sphere; the equator corresponds to the $U(1)$ phase of the SC order parameter while the poles correspond to two possible checkerboard CDW orders. A generic point on the sphere represents coexisting SC and CDW orders. Right: The order parameters forming a "meron" in the vicinity of a vortex, with $t' = 0.3t$. Far from the core, the pseudospins lie in the plane and wind by 2π as we move around the vortex. Within the core, they cant out of the plane to generate CDW order.

considerations, we assert that the Hubbard model is described by the following Landau-Ginzburg free energy density,

$$\mathcal{L} = \frac{\rho}{2}\left|\left(\nabla - \frac{ie}{\hbar c}\mathbf{A}\right)\Delta(\mathbf{r})\right|^2 + \frac{1}{8\pi}(\nabla \times \mathbf{A})^2 + \frac{\rho}{2}|\nabla\tilde{\phi}(\mathbf{r})|^2 - |\Delta(\mathbf{r})|^2 - (1 - gt'^2)|\tilde{\phi}(\mathbf{r})|^2, \quad (2)$$

with the order parameters constrained by the uniform-length constraint. The t' hopping introduces an anisotropy by increasing the energy of the CDW state; when $t' = 0$ and the magnetic field is turned off, we see that SC and CDW orders become degenerate to reveal the underlying $SO(3)$ symmetry. Below, we study the Hubbard model within a mean-field approach and obtain results consistent with this field theory.

Motivated by recent experiments revealing charge order in the cuprates, several studies have considered field theories similar to Eq. (2) [15–17], with Refs. [18,19] also incorporating an orbital magnetic field. Our study demonstrates that the Hubbard model, at strong coupling, provides an ultraviolet regularization of such a field theory. The mean-field results presented below can be viewed as saddle-point solutions of the field theory.

IV. BOGOLIUBOV–DE GENNES MEAN-FIELD THEORY

We study the Hubbard model with the interaction strength fixed at $U = 10t$, as we are interested in the strong-coupling regime. We consider two tuning parameters in the Hamiltonian: the next-nearest-neighbor hopping t' and the orbital field strength (described below). We perform real-space mean-field simulations on an $L \times L$ lattice with periodic boundary conditions, with L up to 30. To introduce an orbital magnetic field, we add a complex phase to the hopping amplitudes t_{ij} given by $\theta_{ij} = e\int_{\mathbf{r_i}}^{\mathbf{r_j}} \mathbf{A}\cdot\mathbf{dr}$, where $\mathbf{A}(\mathbf{r})$ is the vector potential; see Appendix for details. We take the magnetic field to be uniform, assuming strong type II superconductivity ($\kappa \gg 1$). The net magnetic flux through a closed surface must be quantized in units of h/e [20]. We take the net flux through our system to be $\alpha h/e$ where α is an integer. As each vortex carries a flux $\Phi_0 = h/2e$, we will always have an even number of vortices in the system. In particular, the lowest magnetic flux we can have is $2\Phi_0$, corresponding to two vortices.

We decompose the on-site interaction term in pairing and density channels. The SC order parameter is complex-valued, defined as $\Delta_i = U\langle c_{i\downarrow}c_{i\uparrow}\rangle$. The density order parameter is defined as $\phi_i = \frac{U}{2}\langle\hat{n}_{i\uparrow} + \hat{n}_{i\downarrow}\rangle = \frac{U}{2}(\langle c^\dagger_{i\uparrow}c_{i\uparrow}\rangle + \langle c^\dagger_{i\downarrow}c_{i\downarrow}\rangle)$. The local CDW order parameter can be defined as $\tilde{\phi}_i = (-1)^{\mathbf{r}_i}\{\phi_i - U/2\}$, which measures the deviation from half filling. With these mean-field parameters, the Hamiltonian takes the form of a $2L^2 \times 2L^2$ matrix, which can be diagonalized using the Bogoliubov-Valatin transformation [21–23]. We obtain self-consistent values of Δ_i and ϕ_i on every site. All results presented here are obtained at half filling. With our choice of $U = 10t$, we see that mean-field results always satisfy the uniform-length constraint, yielding constant $|\Delta_i|^2 + \tilde{\phi}_i^2$.

We find several self-consistent mean-field configurations, of which the one with lowest energy is to be chosen. One solution is a pure CDW state in which $\Delta_i = 0$ for all i and $\phi_i = \{\phi_0 + (-1)^{\mathbf{r}_i}\tilde{\phi}\}$, corresponding to uniform CDW order. In the absence of a magnetic field and in the presence of a nonzero t', this state has higher energy than the uniform SC phase. When a field is imposed, this state is not affected as it is insulating; its energy remains constant, independent of the flux (see Appendix). In contrast, the SC phase necessarily develops vortices when a field is imposed. As the number of vortices increases with flux, so does the energy of the SC. As seen from these energetic arguments, an applied magnetic field induces competition between SC and CDW orders.

V. RESULTS

A. Vortex profile

Setting $\alpha = 1$, we obtain the lowest flux configuration with two well-separated vortices. As t' is increased, we find CDW order in the vortex core until $t' \lesssim 0.5t$. For larger t' values, we find a normal core with no CDW correlations. Figures 2(a) and 2(b) show the profiles of superconducting and CDW order at selected values of t'. The lower panels of Fig. 2 show the spatial maps of SC and CDW order parameters around a single vortex for $t' = 0.3t$: CDW correlations can be clearly seen in the vortex core region. The same information is presented in spin language in Fig. 1 (right).

The SC and CDW profiles are, in fact, set by the same length scale, ξ, as the order parameters are not independent due to the uniform-spin-length constraint. From our mean-field results, we obtain ξ by fitting the SC profile to $\Delta(x) \sim \Delta_0 \tanh(x/\xi)$, a functional form consistent with the field theory of Eq. (2) [13]. The resulting ξ scales as $1/t'$ as shown in the inset to Fig. 2(a). This is consistent with the field theory which has an inherent length scale, $\xi_{\mathcal{L}} \sim \sqrt{\rho/gt'^2} \sim 1/t'$. This provides strong evidence for the validity of the field theory description.

B. Length scales in the vortex

Although the vortex profile is characterized by a single length scale ξ, we define two lengths, L_Δ and L_ϕ, as the full widths at half maximum of SC and CDW profiles, respectively. We find that both L_Δ and L_ϕ are proportional to ξ. However,

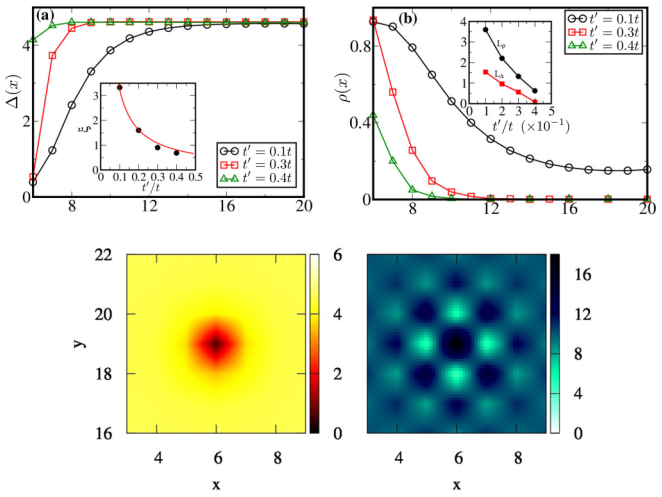

FIG. 2. (a) Superconducting and (b) CDW order profiles at different t'. The inset to panel (a) shows the underlying length scale ξ vs t'. The red line is a fit to $\xi \sim 1/t'$. The inset to panel (b) shows the FWHM widths, L_Δ and L_ρ, vs t'. The lower panels show the spatial maps of SC ($|\Delta_i|$) (left) and density (ϕ_i) (right) order parameters around a vortex core for $t' = 0.3t$. The interaction strength is fixed at $U = 10t$.

L_ϕ is always larger than L_Δ as shown in the inset to Fig. 2(b). This is a direct consequence of the nonlinear constant-squared-sum constraint: while SC reaches half of its asymptotic value quickly, CDW correlations drop to half their value at a longer radius. We argue below that this invariably leads to phase coexistence. The argument goes through in any system with a similar constraint, e.g., the proposed field theory for YBCO in Ref. [16].

As flux is increased, the vortex density increases and the typical intervortex distance, a_{v-v}, shrinks. We expect superconductivity to survive until $a_{v-v} \sim L_\Delta$, a criterion typically used to estimate H_{c2}. However, before we hit this field strength, we encounter another threshold when $a_{v-v} \sim L_\phi$; note that $L_\Delta < L_\phi$. At this point, the CDW regions around each vortex overlap. The CDW order coherently percolates throughout the system on top of the SC background, leading to a supersolid with coexisting orders. Thus, the squared-sum constraint inevitably leads to field-driven phase coexistence. This is elucidated by our mean-field results presented below.

C. Vortex lattice evolution

Figure 3 shows our results for $t' = 0.2t$ on a 24×24 lattice for various α values (the total magnetic flux being $\alpha h/e$). The panels show real-space maps of Δ_i and ϕ_i, showing the evolution of a vortex lattice with increasing flux. In addition, we plot the Fourier transform of the SC order parameter, defined as $S_\Delta(\mathbf{q}) = (1/N)\sum_i |\Delta_i|^2 e^{i\mathbf{q}\cdot\mathbf{r_i}}$. The distribution of peaks in $S_\Delta(\mathbf{q})$ reveals the geometry of the vortex lattice. The figure also shows the electronic density of states in the mean-field ground state.

For small fields, with $\alpha = 2,4$, we find well-separated vortices forming an anisotropic triangular lattice. At $\alpha = 6$, the lattice becomes near isotropic. Upon increasing the field to $\alpha = 8$, the vortices form a square lattice. This suggests an

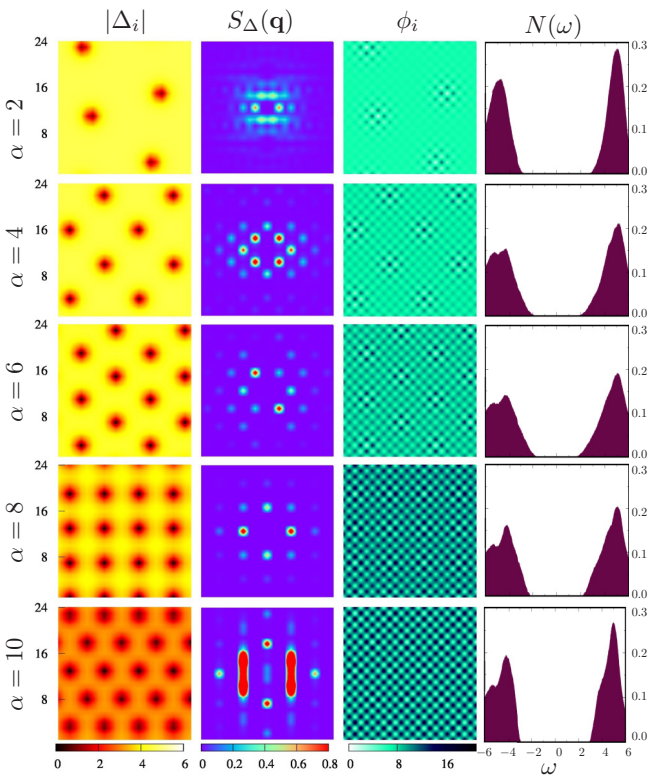

FIG. 3. Spatial maps of the SC order parameter amplitude, Fourier transform of SC amplitude, and the density order parameter. The results are for $L = 24$, $t' = 0.2t$, and five different magnetic field values, parametrized by α. We also show the electronic density of states, $N(\omega)$, as a function of field.

underlying phase transition driven by tuning vortex density. For $\alpha > 8$, we find phase separation into square and triangular vortex lattices. Similar lattice transitions have been seen in YBCO at high fields with triangular-square [24] and square-triangular transitions [25] reported. Finally, at $\alpha = 12$, we find a first-order phase transition to a pure CDW phase, which has lower energy than solutions with SC order. Thus, at mean-field level, H_{c2} is set by the competing CDW phase, unlike in conventional superconductors. A similar transition to a competing phase has been seen in YBCO using thermal conductivity measurements [26].

D. Phase coexistence

The second key result of this work is a field-driven SC-CDW coexistence regime. As seen in Fig. 3, every vortex core nucleates CDW correlations which begin to overlap when $\alpha = 4$. The CDW order becomes progressively stronger with increasing field as vortex cores overlap more and more. For $\alpha \gtrsim 8$, we have near-uniform CDW order. With increasing field, the SC order weakens while the CDW order parameter grows. As a result, the electronic gap never closes, as shown in Fig. 3.

Figure 4(a) shows the in-field phase diagram for $t' = 0.2t$. As we force a magnetic flux through Peierl's substitution, there is no H_{c1} in our simulations. To quantify the strength of CDW order, we define $\rho = \rho_{(\pi,\pi)}/\rho_{(0,0)}$ where $\rho_{\mathbf{q}}$ is the

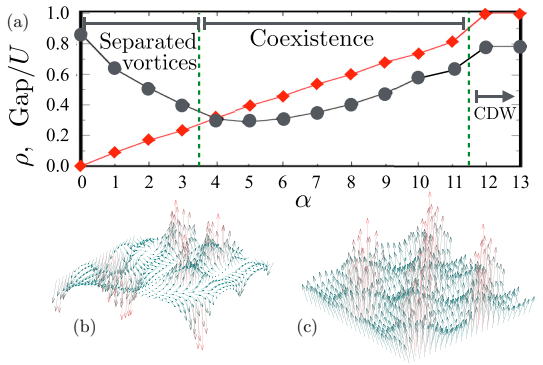

FIG. 4. (a) CDW parameter ρ (red diamonds) and the quasiparticle gap (gray circles) as a function of flux α at $t' = 0.2t$. The CDW regions around vortex cores begin to overlap at $\alpha = 4$, heralding coexistence. The gap starts to increase beyond this threshold. In the high-field "CDW" region, a pure CDW mean-field state is favored over a SC phase. (b), (c) The pseudospin texture at $\alpha = 3$ and 4—before and after CDW correlations span the system. The z component of spins orders coherently in the coexistence phase.

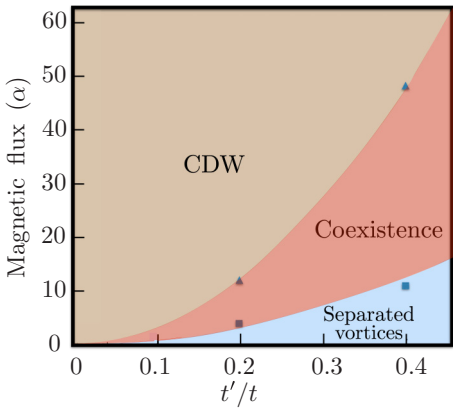

FIG. 5. Mean-field phase diagram in the t'-α plane. Phase boundaries are fits to the form $\alpha_c \sim t'^2$ (see text). The lower boundary marks the threshold field at which CDW correlations begin to span the system. The upper boundary corresponds to H_{c2}, a first-order phase transition into a pure CDW state.

Fourier component of the density: $\rho_{\mathbf{q}} = \sum_i \phi_i e^{i\mathbf{q}\cdot\mathbf{r}_i}$. In a perfect CDW state with site occupation oscillating between 0 and 2, ρ is unity. For small α values, we find ρ to be small, indicating weak CDW order arising from well-separated vortex cores. The CDW puddles formed in the cores are not necessarily in-phase; each puddle independently chooses one of the two checkerboard CDW patterns. With increasing α, ρ increases monotonically. When $\rho \sim 0.3$, we find that CDW correlations begin to span the entire system. Consequently, the system spontaneously picks one of the two CDW orders. This marks the onset of supersolidity. Our calculations of superfluid stiffness indicate that supersolidity is stable to fluctuations (see Appendix). In pseudospin language, the supersolid corresponds to a "meron crystal" with a $\mathbb{Z}_2$ broken symmetry, corresponding to choice of ordering along the $\pm\hat{z}$ direction; see Fig. 4(c).

While CDW and SC compete spatially, they both serve to open an electronic gap. At zero field, we have a uniform SC state with a large gap of the order of U. An applied field introduces vortices with CDW correlations, leading to a spatially textured $SO(3)$ order parameter field. For small magnetic fields, these order parameter gradients reduce the electronic gap. Once CDW order percolates throughout the system, the CDW order parameter no longer suffers sharp gradients and strengthens the gap once again.

E. Phase diagram

Figure 5 shows the phase diagram for the Hubbard model in the t'-α plane. We restrict ourselves to $t' \lesssim 0.5t$, the region with charge-ordered vortex cores. There are two phase boundaries here: (a) the onset of phase coexistence and (b) H_{c2}. The shape of these curves is given by the following qualitative argument.

With increasing flux, the vortex density increases. Consequently, the typical intervortex distance shrinks as $a_{v-v} \sim \alpha^{-1/2}$. On the other hand, each vortex has two associated radii, L_Δ and L_ϕ. Superconductivity is suppressed out to a radius set by L_Δ, while CDW correlations extend to a larger distance, L_ϕ. Both these distances are proportional to the vortex length scale $\xi \sim 1/t'$, with $L_\Delta < L_\phi$.

Phase coexistence sets in when CDW correlations overlap, i.e., $a_{v-v} \sim L_\phi$. Using the scaling of a_{v-v} and L_ϕ obtained above, we find $\alpha_{\text{coex.}} \sim t'^2$. Similarly, H_{c2} occurs when $a_{v-v} \sim L_\Delta$, which gives $\alpha_{c2} \sim t'^2$. Our mean-field results are consistent with these relations, with phase boundaries well described by $\alpha_{c2/\text{coex}} \sim t'^2$.

VI. DISCUSSION

In the context of the attractive Hubbard model, we have shown that competing CDW order emerges in vortex cores. Furthermore, we have demonstrated a field-driven SC-CDW coexistence regime arising from overlap of vortex cores. This state simultaneously breaks translational symmetry and $U(1)$ gauge symmetry, forming a "supersolid" [27]. Despite several theoretical proposals [28–32] and suggestive signatures in liquid He experiments [27], no unambiguous experimental realization of supersolidity has been found to date. Our study suggests that superconductors with competing phases are strong candidates to realize supersolidity.

Our strong-coupling mean-field theory can be seen as a pseudospin problem with chiral interactions introduced by the orbital magnetic field. Our work provides a demonstration of a "meron crystal"—a spin state with chiral texture [33]. A close analog, the skyrmion crystal, has seen a surge of interest recently [34]. Variants of skyrmion crystals with ordered arrangements of merons and antimerons have been proposed earlier [35,36]. In contrast, we have demonstrated a solid consisting solely of merons. Several phenomena seen in skyrmion crystals, such as electromagnetic control, thermal Hall effect, etc., may also appear in meron crystals.

At large magnetic fields, CDW order becomes much stronger than SC. In this regime, fluctuations may destabilize SC while leaving the CDW order intact. This suggests a "vortex liquid" phase with remnant CDW order and vanishing

superfluid stiffness. This is an exciting direction for future study with interesting implications for the cuprates [37–39].

Our results broadly apply to several material families which host competing orders. We have used t' as a knob to tune phase competition; this role could be played by experimentally tunable parameters such as doping in the cuprates [2], pressure in $TiSe_2$ [40], etc. Our results provide a theoretical paradigm to understand phase competition in these systems.

ACKNOWLEDGMENTS

We thank Arun Paramekanti, David Hawthorn, David Broun, and Anton Burkov for discussions. M.K. acknowledges the use of the High Performance Computing Facility at Harish Chandra Research Institute, Allahabad, India.

APPENDIX

1. Peierl's substitution

We have two types of hopping terms in our Hamiltonian: nearest-neighbor hopping with amplitude t and next-nearest-neighbor hopping with amplitude t'. The phase of each hopping element represents a line integral of the vector potential, in accordance with the principle of Peierl's substitution. As the vector potential is not uniquely defined, there are several possible ways to assign the complex phases. The gauge-invariant quantity is the magnetic flux: the sum of the hopping phases along closed loops on the lattice.

In our periodic $L \times L$ lattice, we assign hopping phases so as to obtain a uniform magnetic flux. We use the scheme shown in Fig. 6. We have introduced a parameter ϕ which encodes the phase picked up by an electron when hopping around any square plaquette; i.e., the magnetic flux through each square plaquette is $\hbar\phi/e$. Our square lattice system with periodic boundary conditions is equivalent to a torus, a closed surface. As shown by Dirac, the magnetic flux through any closed surface must be quantized in units of h/e so that $\phi = 2\alpha\pi/L^2$,

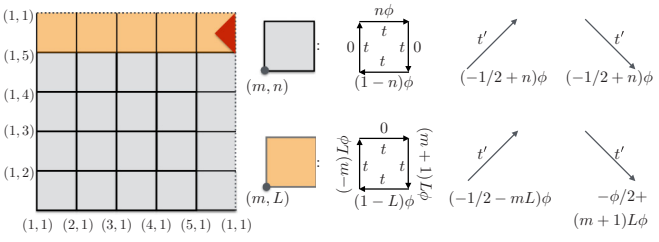

FIG. 6. Peierls substitution scheme on the $L \times L$ lattice. Left: The periodic cluster for $L = 5$ for illustration purposes. Sites are labeled as (m,n); not all site labels are shown. The bonds present in the cluster are depicted using dark solid lines. Bonds repeated due to periodic boundary conditions are shown in dotted lines. The square plaquettes are divided into two types as indicated by the color. Right: Representative plaquettes of each type are shown, with the lower-left site labeled. The hopping phases for the bonds on these plaquettes are shown. The parameter ϕ determines the flux through each square plaquette, given by $\hbar\phi/e$. The Dirac string passes through the red triangular area. Due to the Dirac string, the flux is constrained to satisfy $\phi = 2\alpha\pi/L^2$, where α is an integer.

with α being an integer. The parameter α determines the total flux through the system, given by $\alpha h/e$.

Dirac further argued that in the presence of a nonzero flux, we cannot define electronic wave functions on the surface smoothly. The phase of the wave functions must wind around a singularity, which is called the "Dirac string." In our scheme, the Dirac string passes through the red region within the top-right square plaquette in Fig. 6. The sum of the hopping phases around a contour which encloses this region has an additional contribution of $L^2\phi = 2\pi\alpha$. This does not indicate an increased magnetic flux through this region; rather, it reflects a singularity in the definition of the electronic wave functions. Indeed, as this phase is a multiple of 2π, it does not lead to any observable consequences.

2. Bogoliubov–de Gennes formalism

The Hamiltonian for the Hubbard model is given in the main text. We decompose the on-site interaction term in pairing and density channels via a mean-field decomposition. The complex superconducting order parameter is defined as $\Delta_i = U\langle c_{i\downarrow}c_{i\uparrow}\rangle$, while the charge order parameter is defined as $\phi_i = \frac{U}{2}(n_{i\uparrow} + n_{i\downarrow}) = \frac{U}{2}(\langle c^\dagger_{i\uparrow}c_{i\uparrow}\rangle + \langle c^\dagger_{i\downarrow}c_{i\downarrow}\rangle)$. The resulting effective Hamiltonian is given by

$$\begin{aligned} H_{MFT} = &-t\sum_{\langle ij\rangle,\sigma} e^{i\theta_{ij}} c^\dagger_{i\sigma}c_{j\sigma} - t'\sum_{\langle\langle ij\rangle\rangle,\sigma} e^{i\chi_{ij}} c^\dagger_{i\sigma}c_{j\sigma} + \text{H.c.} \\ &- \sum_{i,\sigma}\{\mu + \phi_i\}c^\dagger_{i\sigma}c_{i\sigma} - \sum_i(\Delta_i c^\dagger_{i\uparrow}c^\dagger_{i\downarrow} + \Delta^*_i c_{i\uparrow}c_{i\downarrow}) \\ &+ \sum_i\{|\Delta_i|^2 + \phi_i^2\}/|U|. \end{aligned} \tag{A1}$$

The hopping phases θ_{ij} and χ_{ij} are assigned according to the Peierl's substitution scheme described above. We diagonalize this Hamiltonian using a Bogoliubov-Valatin transformation given by $c_{i\sigma} = \sum_m(u_{mi\sigma}\gamma_{m\sigma} - s_\sigma v^*_{mi\sigma}\gamma^\dagger_{m,-\sigma})$, where $\gamma^\dagger_{m\sigma}$ ($\gamma_{m\sigma}$) creates (annihilates) a quasiparticle with spin σ with energy ϵ^σ_m and wave functions $u_{mi\sigma}$ and $v_{mi\sigma}$. We have introduced a spin index $s_\uparrow = 1$ and $s_\downarrow = -1$. The resulting gap and number equations are

$$\begin{aligned} \Delta_i &= U\sum_m\{v^*_{mi\downarrow}u_{mi\uparrow}f(\epsilon_{m\uparrow}) + u^*_{mi\downarrow}v_{mi\uparrow}f(\epsilon_{m\downarrow})\}, \\ n_{i\uparrow} &= \sum_m\{|u_{mi\uparrow}|^2 f(\epsilon_{m\uparrow}) + |v_{mi\uparrow}|^2 f(\epsilon_{m\downarrow})\}, \\ n_{i\downarrow} &= \sum_m\{|u_{mi\downarrow}|^2[1 - f(\epsilon_{m\uparrow})] + |v_{mi\downarrow}|^2[1 - f(\epsilon_{m\downarrow})]\}, \end{aligned} \tag{A2}$$

where $f(\epsilon_m) = 1$ (0) if $\epsilon_m < 0$ (> 0) is the Fermi function at zero temperature. Starting from initial guess values, we iterate these equations to obtain self-consistent values of Δ_i and ϕ_i. The chemical potential is tuned to fix the density at half filling.

3. Phase competition

For a given set of parameters t', U, and α, we find several self-consistent solutions. In particular, we find a pure CDW state with $\Delta_i = 0$. To illustrate the phase competition in the

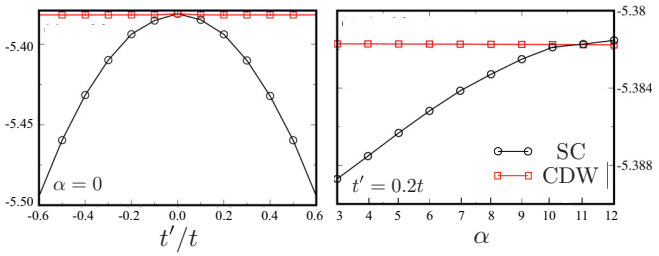

FIG. 7. Phase competition between SC and CDW orders. Left: Comparison of ground-state energies as a function of t'/t, with the magnetic field turned off ($\alpha = 0$). At $t' = 0$, the two orders are degenerate. A nonzero value of t' lowers the energy of the SC state. Right: Ground-state energies as a function of magnetic flux, α, with t' fixed at $0.2t$. At $\alpha = 12$, the CDW state wins over the SC state indicating a first-order phase transition. All energies are calculated at half filling.

Hubbard model, we compare the energy of this CDW state with that of the SC state in Fig. 7. In the absence of a magnetic field ($\alpha = 0$), the two states are degenerate when $t' = 0$, while a nonzero t' lowers the energy of the SC state.

Competition between orders can also be tuned by increasing the magnetic field. This is depicted in Fig. 7 (right). When α is increased at fixed t', the energy of the CDW state does not change as the CDW state is an insulator. However, in the SC phase, increasing α introduces more vortices and increases the energy. The energy of the SC state steadily rises and eventually crosses the CDW energy. This signals H_{c2} at the mean-field level, with CDW order becoming energetically favorable over a superconducting vortex state.

4. Higher-t' regime

With increasing t', the radius of the CDW region in each vortex core shrinks. Consequently, the threshold field for coexistence increases. Figure 8 shows spatial maps of the SC and CDW order parameters for $t' = 0.4t$ which can be compared with the $t' = 0.2t$ data in Fig. 3 of the main text. The percolation of CDW correlations is slow to occur with a coexistence state only setting at $\alpha \sim 11$. Finally, H_{c2} is encountered at $\alpha \sim 48$, when the CDW state becomes energetically favorable. Unlike the case of $t' = 0.2$ discussed in the main text, it is difficult to discern changes in the geometry of the vortex lattice here due to the high density of vortices.

5. Superfluid stiffness

Our mean-field results indicate coexistence of SC and CDW orders, forming a supersolid state. To check whether this phase is stable to fluctuations, the standard diagnostic is superfluid stiffness, which measures the energy cost of imposing a smooth gradient in the SC order parameter. To estimate the stiffness, we take the following route. We introduce an additional component of the vector potential $\mathbf{A}_{\text{tangential}} = 2\pi\hat{x}/L$. If we were to turn off the orbital magnetic field, this vector potential leads to a "flowing" superfluid solution with $\Delta_i \sim \Delta_0 e^{i4\pi x_i/L}$. The resulting energy cost is a measure of superfluid stiffness. For a simple superfluid with no competing order, this energy cost (the increase in energy per site) is proportional to ρ/L^2, where ρ is the superfluid stiffness and L is the system size. We define $\eta(L) = E_{2\pi} - E_0$, where $E_{2\pi}$ is the energy (per site) of the flowing state. This is calculated by using the Δ_i values obtained after inclusion of the tangential vector potential to evaluate the expectation value of the mean-field Hamiltonian.

The obtained $\eta(L)$ values are plotted as a function of $1/L^2$ in Fig. 9. In the $\alpha = 0$ case (no orbital magnetic field), we see that $\eta(L)$ indeed scales as $1/L^2$, with a positive slope. This slope is proportional to the superfluid stiffness.

In the presence of the orbital field, we seek to plot $\eta(L)$ for configurations with the same magnetic flux density across different system sizes. In our calculations, the magnetic flux density is $\alpha h/eL^2$, with α being an integer and L ranging from 18–30 (for smaller sizes, we see strong finite-size effects). Generically, it is not possible to find multiple $\{\alpha, L\}$ values for which α/L^2 is a constant. In Fig. 9, we plot $\eta(L)$ for $\{\alpha, L\} = (\{2,18\},\{4,24\},\{6,30\})$ and $(\{4,18\},\{8,24\},\{12,30\})$ which correspond to approximately constant α/L^2 values. The resulting $\eta(L)$ values also scale linearly with $1/L^2$ with a positive slope. We conclude that the superfluid stiffness is positive for these flux densities. We also note that the stiffness

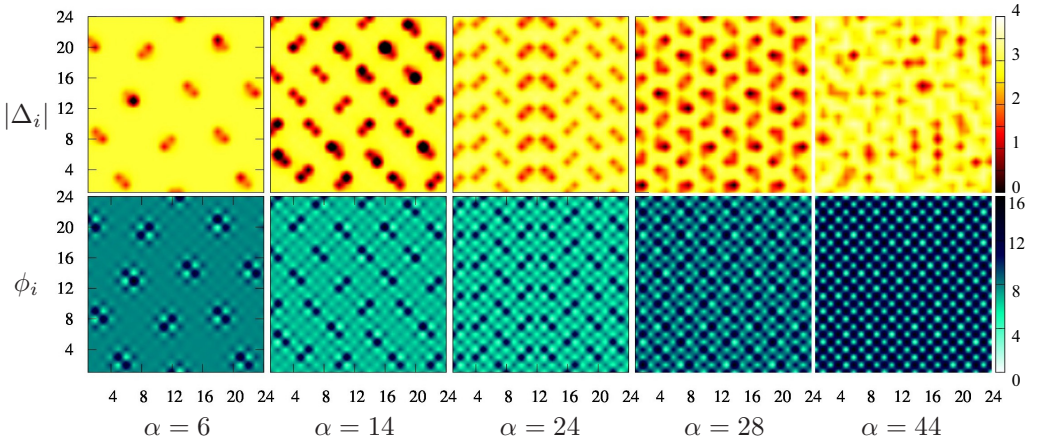

FIG. 8. Spatial maps of the pairing amplitude ($|\Delta_i|$) and the CDW (ϕ_i) order with changing magnetic field at $t' = 0.4t$ on a 24×24 lattice.

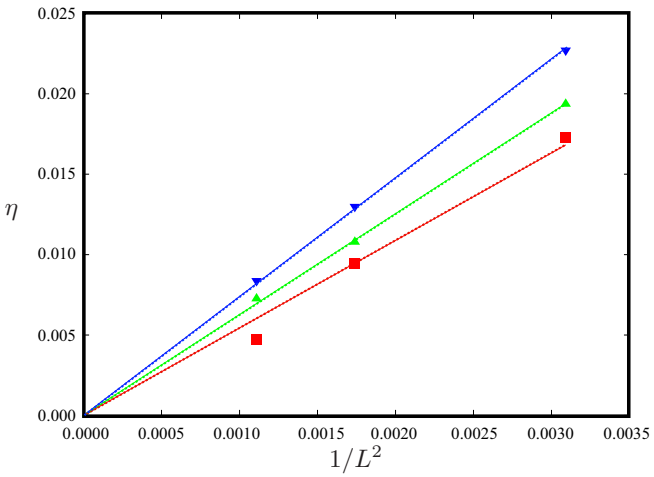

FIG. 9. Superfluid stiffness. We plot $\eta(L)$ vs $1/L^2$ for three sets of $\{\alpha, L\}$ values: (a) ($\{0,18\},\{0,24\},\{0,30\}$) (blue downward triangles), (b) ($\{2,18\},\{4,24\},\{6,30\}$) (green upward triangles), and (c) ($\{4,18\},\{8,24\},\{12,30\}$) (red squares). The lines are fits to the form $\eta = \rho/L^2$. All three best-fit lines have positive slopes indicating a positive superfluid stiffness.

decreases with increasing flux density. In particular, we note that the stiffness is positive for the flux densities corresponding to $\alpha = 4$ and $\alpha = 8$ on a 24×24 lattice. As discussed in the main text, these parameters have macroscopic CDW order with CDW correlations spanning the entire system. This suggests that the coexistence phase is stable to fluctuations.

It is possible that that stiffness may vanish at higher flux densities, perhaps close to H_{c2}. In this regime, the CDW order parameter becomes approximately constant while the SC order parameter suffers large gradients due to the presence of vortices. It is then conceivable that fluctuations can wash out the in-plane order while preserving order in the z direction. This will lead to a "pairing liquid" state (analogous to a spin liquid) with remnant CDW ordering. Equivalently, this can be understood as melting of the vortex lattice. Below this threshold, the intervortex distances are fixed by strong interactions between vortices. A small amount of disorder will then suffice to pin the entire vortex lattice so as to generate a robust SC state. However, when fluctuations wash out the coherence in the SC, the vortices become mobile giving rise to a "vortex liquid." This is an interesting direction for future study.

[1] B. Lake, G. Aeppli, K. N. Clausen, D. F. McMorrow, K. Lefmann, N. E. Hussey, N. Mangkorntong, M. Nohara, H. Takagi, T. E. Mason, and A. Schröder, Science **291**, 1759 (2001).

[2] J. Chang, E. Blackburn, A. T. Holmes, N. B. Christensen, J. Larsen, J. Mesot, R. Liang, D. A. Bonn, W. N. Hardy, A. Watenphul, M. v. Zimmermann, E. M. Forgan, and S. M. Hayden, Nat. Phys. **8**, 871 (2012).

[3] J. E. Hoffman, E. W. Hudson, K. M. Lang, V. Madhavan, H. Eisaki, S. Uchida, and J. C. Davis, Science **295**, 466 (2002).

[4] P. J. Curran, V. V. Khotkevych, S. J. Bending, A. S. Gibbs, S. L. Lee, and A. P. Mackenzie, Phys. Rev. B **84**, 104507 (2011).

[5] T. Machida, Y. Kohsaka, K. Matsuoka, K. Iwaya, T. Hanaguri, and T. Tamegai, Nat. Commun. **7**, 11747 (2016).

[6] T. Wu, H. Mayaffre, S. Krämer, M. Horvatić, C. Berthier, P. L. Kuhns, A. P. Reyes, R. Liang, W. N. Hardy, D. A. Bonn, and M.-H. Julien, Nat. Commun. **4**, 2113 (2013).

[7] C. N. Yang, Phys. Rev. Lett. **63**, 2144 (1989).

[8] S. Zhang, Phys. Rev. Lett. **65**, 120 (1990).

[9] C. N. Yang and S. C. Zhang, Mod. Phys. Lett. B **04**, 759 (1990).

[10] A. A. Burkov and A. Paramekanti, Phys. Rev. Lett. **100**, 255301 (2008).

[11] R. Ganesh, A. Paramekanti, and A. A. Burkov, Phys. Rev. A **80**, 043612 (2009).

[12] E. Demler, W. Hanke, and S.-C. Zhang, Rev. Mod. Phys. **76**, 909 (2004).

[13] D. P. Arovas, A. J. Berlinsky, C. Kallin, and S.-C. Zhang, Phys. Rev. Lett. **79**, 2871 (1997).

[14] J.-P. Hu and S.-C. Zhang, J. Phys. Chem. Solids **63**, 2277 (2002).

[15] K. B. Efetov, H. Meier, and C. Pepin, Nat. Phys. **9**, 442 (2013).

[16] L. E. Hayward, D. G. Hawthorn, R. G. Melko, and S. Sachdev, Science **343**, 1336 (2014).

[17] G. Wachtel and D. Orgad, Phys. Rev. B **90**, 224506 (2014).

[18] H. Meier, M. Einenkel, C. Pépin, and K. B. Efetov, Phys. Rev. B **88**, 020506 (2013).

[19] Y. Caplan and D. Orgad, Phys. Rev. Lett. **119**, 107002 (2017).

[20] P. A. M. Dirac, Proc. R. Soc. London A **133**, 60 (1931).

[21] Y. Chen and C. S. Ting, Phys. Rev. B **65**, 180513 (2002).

[22] H.-Y. Chen and C. S. Ting, Phys. Rev. B **71**, 220510 (2005).

[23] Q. Han, J. Phys.: Condens. Matter **22**, 035702 (2010).

[24] S. P. Brown, D. Charalambous, E. C. Jones, E. M. Forgan, P. G. Kealey, A. Erb, and J. Kohlbrecher, Phys. Rev. Lett. **92**, 067004 (2004).

[25] J. S. White, S. P. Brown, E. M. Forgan, M. Laver, C. J. Bowell, R. J. Lycett, D. Charalambous, V. Hinkov, A. Erb, and J. Kohlbrecher, Phys. Rev. B **78**, 174513 (2008).

[26] G. Grissonnanche, O. Cyr-Choinière, F. Laliberté, S. Renéde Cotret, A. Juneau-Fecteau, S. Dufour-Beauséjour, M. È. Delage, D. LeBoeuf, J. Chang, B. J. Ramshaw, D. A. Bonn, W. N. Hardy, R. Liang, S. Adachi, N. E. Hussey, B. Vignolle, C. Proust, M. Sutherland, S. Krämer, J. H. Park, D. Graf, N. Doiron-Leyraud, and L. Taillefer, Nat. Commun. **5**, 3280 (2014).

[27] M. Boninsegni and N. V. Prokof'ev, Rev. Mod. Phys. **84**, 759 (2012).

[28] G. G. Batrouni and R. T. Scalettar, Phys. Rev. Lett. **84**, 1599 (2000).

[29] F. Hébert, G. G. Batrouni, R. T. Scalettar, G. Schmid, M. Troyer, and A. Dorneich, Phys. Rev. B **65**, 014513 (2001).

[30] R. G. Melko, A. Paramekanti, A. A. Burkov, A. Vishwanath, D. N. Sheng, and L. Balents, Phys. Rev. Lett. **95**, 127207 (2005).

[31] S. Wessel and M. Troyer, Phys. Rev. Lett. **95**, 127205 (2005).

[32] L. Pollet, J. D. Picon, H. P. Büchler, and M. Troyer, Phys. Rev. Lett. **104**, 125302 (2010).

[33] G. E. Volovik and M. Krusius, Physics **5**, 130 (2012).

[34] N. Nagaosa and Y. Tokura, Nat. Nanotechnol. **8**, 899 (2013).
[35] L. Brey, H. A. Fertig, R. Côté, and A. H. MacDonald, Phys. Scr. **T66**, 154 (1996).
[36] R. Côté, W. Luo, B. Petrov, Y. Barlas, and A. H. MacDonald, Phys. Rev. B **82**, 245307 (2010).
[37] D. LeBoeuf, S. Kramer, W. N. Hardy, R. Liang, D. A. Bonn, and C. Proust, Nat. Phys. **9**, 79 (2013).
[38] S. Gerber, H. Jang, H. Nojiri, S. Matsuzawa, H. Yasumura, D. A. Bonn, R. Liang, W. N. Hardy, Z. Islam, A. Mehta, S. Song, M. Sikorski, D. Stefanescu, Y. Feng, S. A. Kivelson, T. P. Devereaux, Z.-X. Shen, C.-C. Kao, W.-S. Lee, D. Zhu, and J.-S. Lee, Science **350**, 949 (2015).
[39] F. Yu, M. Hirschberger, T. Loew, G. Li, B. J. Lawson, T. Asaba, J. B. Kemper, T. Liang, J. Porras, G. S. Boebinger, J. Singleton, B. Keimer, L. Li, and N. P. Ong, Proc. Natl. Acad. Sci. U.S.A. **113**, 12667 (2016).
[40] A. F. Kusmartseva, B. Sipos, H. Berger, L. Forró, and E. Tutiš, Phys. Rev. Lett. **103**, 236401 (2009).